

SOLAR-LIKE OSCILLATIONS IN α CENTAURI B

HANS KJELSDSEN,¹ TIMOTHY R. BEDDING,² R. PAUL BUTLER,³ JØRGEN CHRISTENSEN-DALSGAARD,¹ LASZLO L. KISS,²
CHRIS MCCARTHY,³ GEOFFREY W. MARCY,⁴ CHRISTOPHER G. TINNEY,⁵ AND JASON T. WRIGHT⁴

Received 2005 April 7; accepted 2005 August 26

ABSTRACT

We have made velocity observations of the star α Centauri B from two sites, allowing us to identify 37 oscillation modes with $l = 0-3$. Fitting to these modes gives the large and small frequency separations as a function of frequency. The mode lifetime, as measured from the scatter of the oscillation frequencies about a smooth trend, is similar to that in the Sun. Limited observations of the star δ Pav show oscillations centered at 2.3 mHz, with peak amplitudes close to solar. We introduce a new method of measuring oscillation amplitudes from heavily smoothed power density spectra, from which we estimated amplitudes for α Cen α and B, β Hyi, δ Pav, and the Sun. We point out that the oscillation amplitudes may depend on which spectral lines are used for the velocity measurements.

Subject headings: stars: individual (α Centauri A, α Centauri B, β Hydri, δ Pavonis) — stars: oscillations — Sun: helioseismology

1. INTRODUCTION

The α Centauri A/B system is an excellent target for asteroseismology. Velocity oscillations in the A component were measured by Bouchy & Carrier (2001, 2002) and subsequently by Butler et al. (2004; see also Bedding et al. 2004). The first detection of oscillations in α Cen B (HR 5460) was made by Carrier & Bourban (2003), based on velocity measurements with the CORALIE spectrograph in Chile spanning 13 nights. They observed excess power centered at 4 mHz and used the auto-correlation of the power spectrum to measure a large separation of 161.1 μ Hz. They identified 12 oscillation frequencies with $l = 0-2$, although the high sidelobes from their single-site observations, coupled with the relatively low signal-to-noise ratio (S/N; 2.5–3.5), mean that these may have been affected by daily aliases. Theoretical modeling of α Cen A and B has been carried out several times, most recently by Eggenberger et al. (2004), who also give a thorough review of previous work. Here we report observations of α Cen B made from two sites that show oscillations clearly and allow us to measure their frequencies, amplitudes, and mode lifetimes.

2. VELOCITY OBSERVATIONS AND POWER SPECTRA

We observed α Cen B in 2003 May. At the European Southern Observatory in Chile we used UVES (UV-Visual Echelle Spectrograph) at the 8.2 m Unit Telescope 2 of the Very Large Telescope (VLT).⁶ At Siding Spring Observatory in Australia we used UCLES (University College London Echelle Spectrograph) at the 3.9 m Anglo-Australian Telescope (AAT). In both cases, an

iodine cell was used to provide a stable wavelength reference (Butler et al. 1996).

At the VLT we obtained 3379 spectra of α Cen B, with typical exposure times of 4 s and a median cadence of one exposure every 32 s. At the AAT we obtained 1642 spectra, with typical exposure times of 10–12 s (but sometimes as long as 30 s in poor weather) and a median cadence of one exposure every 91 s. Note that, unlike for our observations of α Cen A, UCLES was used in standard planet-search mode. For α Cen A we rotated the CCD by 90° to speed up readout time, but found that this introduced drifts and sudden jumps in the velocities that we believe are related to the movement of the CCD Dewar as liquid nitrogen boiled off and was refilled (Butler et al. 2004).

The resulting velocities are shown in Figure 1, and the effects of bad weather can be seen (we were allocated five nights with the VLT and eight with the AAT). Both sets of velocities show trends during each night that are presumably due to a combination of instrumental drift and stellar convection noise. To remove these trends, we have subtracted a smoothed version of the data one night at a time, producing the detrended time series shown in Figure 1. This process of high-pass filtering is not strictly necessary, but it does slightly reduce the noise leaking into higher frequencies that would otherwise degrade the oscillation spectrum.

Note that Fourier analysis on unevenly spaced data cannot use the fast Fourier transform (FFT) algorithm. We instead employed the method used for many years by various groups, including our own: we calculated the discrete Fourier transform, but with individual data points being weighted according to their quality (e.g., Deeming 1975; Frandsen et al. 1995).

For about 1 hr at the end of each night, when α Cen B was inaccessible, we observed the star δ Pav (HR 7665; HIP 99240; G8 V). We obtained a total of 179 spectra with the VLT (median cadence 58 s) and 77 with the AAT (median cadence 181 s). The velocities are shown in Figure 2, and there is a clear periodicity of about 7 minutes. We did not expect to be able to measure frequencies with such a limited data set, but we do see a clear excess in the power spectrum from the oscillations (Fig. 3), whose amplitudes we discuss in § 5.

Our analysis of the velocities for α Cen B follows the method that we developed for α Cen A (Butler et al. 2004). We have used the measurement uncertainties, σ_i , as weights in calculating the power spectrum (according to $w_i = 1/\sigma_i^2$), but modified some

¹ Department of Physics and Astronomy, University of Aarhus, DK-8000 Aarhus C, Denmark; hans@phys.au.dk, jcd@phys.au.dk.

² School of Physics A28, University of Sydney, NSW 2006, Australia; bedding@physics.usyd.edu.au, laszlo@physics.usyd.edu.au.

³ Carnegie Institution of Washington, Department of Terrestrial Magnetism, 5241 Broad Branch Road NW, Washington, DC 20015-1305; paul@dtm.ciw.edu, chris@dtm.ciw.edu.

⁴ Department of Astronomy, University of California, Berkeley, CA 94720; and Department of Physics and Astronomy, San Francisco, CA 94132; gmarcy@astron.berkeley.edu.

⁵ Anglo-Australian Observatory, P.O. Box 296, Epping, NSW 1710, Australia; cgt@aaopp.aao.gov.au.

⁶ Based on observations collected at the European Southern Observatory, Paranal, Chile (ESO Programme 71.D-0618).

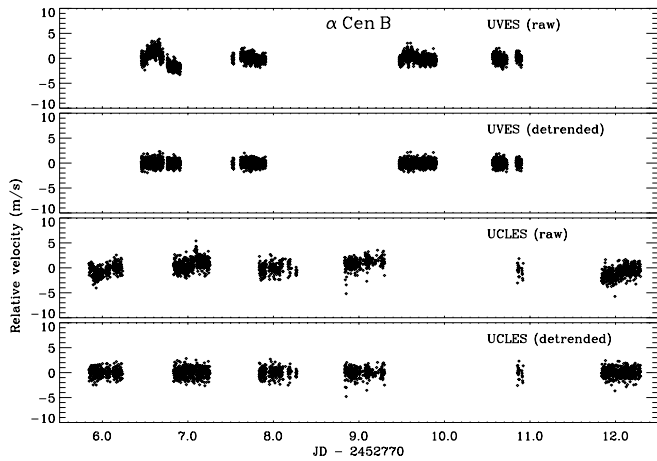


FIG. 1.—Time series of velocity measurements of α Cen B, both before and after removal of slow trends.

of the weights to account for a small fraction of bad data points. In this case, only three data points from UVES and none from UCLES needed to be down-weighted. After these adjustments, we measured the average noise in the amplitude spectrum at high frequencies (above the stellar signal) to be 1.49 cm s^{-1} for UVES (6–8 mHz) and 4.28 cm s^{-1} for UCLES (4.75–5.50 mHz). Note that we used a lower frequency range to measure the noise in the UCLES data because the sampling time of those observations was significantly longer than for UVES (see above).

The power spectrum of the combined series is shown in Figure 4 (*top*). We refer to this as the noise-optimized power spectrum because the weights have been chosen to minimize the noise. The noise level in amplitude is 1.39 cm s^{-1} (6–8 mHz). As such, these measurements replace our observations of α Cen A (1.9 cm s^{-1}) as the most precise amplitude spectrum obtained on any star apart from the Sun.

Figure 4 (*middle*) shows a close-up of the noise-optimized power spectrum. There is a clear series of regular peaks with a spacing of about $81 \mu\text{Hz}$, and we therefore confirm that the large separation is about $162 \mu\text{Hz}$, in agreement with the value reported by Carrier & Bourban (2003). The inset shows the spectral window, in which we see prominent sidelobes (38% in power), due to gaps in the observing window.

As for α Cen A, we have also generated a power spectrum in which the weights were adjusted on a night-by-night basis in order to minimize the sidelobes. The result, which we refer to as the sidelobe-optimized power spectrum, is shown in Figure 4 (*bottom*). The values for these weight multipliers were 5.2 for all UCLES nights except the last, which had 8.4, and 0.5, 0.5, 1.0, and 1.0 for the four UVES nights. Adjusting the weights in this way increased the noise level to 2.40 cm s^{-1} (6–8 mHz), but allowed us to identify correctly peaks that might otherwise be obscured by sidelobes from their stronger neighbors (now reduced to 13% in power). In addition, the sidelobe minimization has slightly improved the frequency resolution, with the FWHM of the spectral window decreasing by about 20% (from 1.83 to $1.44 \mu\text{Hz}$). This is because of the increased weight given to the UCLES data, which covers the longer time span. Note that the dotted lines in Figure 4 show our final oscillation frequencies, which are discussed in detail in § 3.

3. OSCILLATION FREQUENCIES

We measured the frequencies of the strongest peaks in the power spectrum in the standard way, using iterative sine wave

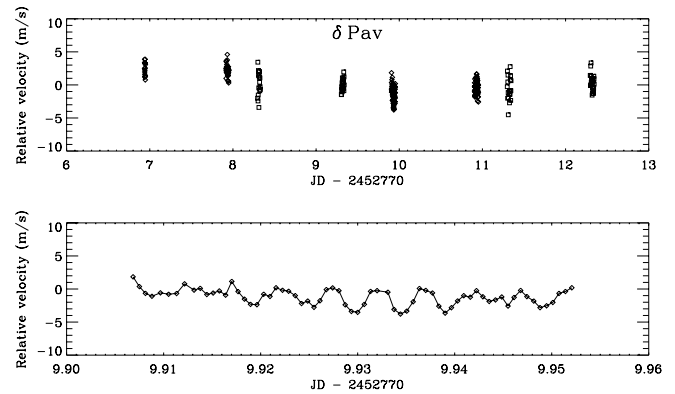


FIG. 2.—Time series of velocity measurements of δ Pav from UVES (*diamonds*) and UCLES (*squares*). *Bottom*: 1.1 hr segment of UVES velocities, in which the 7 minute periodicity is clearly visible.

fitting. We did this for both the noise-optimized and the sidelobe-optimized power spectra, and the resulting frequencies are plotted in echelle format in Figure 5. The echelle format takes advantage of the fact that mode frequencies for low-degree p -mode oscillations are approximated reasonably well by the asymptotic relation:

$$\nu_{n,l} = \Delta\nu \left(n + \frac{1}{2}l + \epsilon \right) - l(l+1)D_0, \quad (1)$$

where n (the radial order) and l (the angular degree) are integers, $\Delta\nu$ (the large separation) reflects the average stellar density, D_0 is sensitive to the sound speed near the core, and ϵ is sensitive to the surface layers.

Symbol size in Figure 5 indicates the S/N of the peaks, and all peaks with $S/N \geq 2.5$ are shown. Many of these represent oscillations, but some are artifacts due to the nonlinear nature of the iterative fitting method and its interaction with noise. The dotted lines represent a fit to the final frequencies that is discussed below; in this figure, they serve to guide the eye and allow us to identify ridges with angular degrees of $l = 0, 1, 2$, and 3.

We can see from Figure 5 that many peaks were identified in both versions of the power spectrum, and, not surprisingly, many were only above $S/N = 2.5$ in the noise-optimized version. However, four peaks that were only significant in the sidelobe-optimized version lie close to the oscillation ridges (three with $l = 0$ and one with $l = 1$). The detection of these peaks vindicates our decision to examine the sidelobe-optimized power spectrum.

The next step was to select those peaks that we believe are due to oscillations and reject those due to noise. This is the only subjective part of the process, but it is required if we are to measure as many frequencies as possible from our data because at this S/N, not all the extracted peaks are genuine. Our final set of identified modes is shown in Figure 6 and Table 1 (and also indicated by the dotted lines in Fig. 4). In some cases the iterative sine wave-fitting produced two peaks (in one case, three) that appear to arise from a single oscillation mode, which is to be expected if we have partially resolved the modes (see § 4 for discussion of the mode lifetimes). In these cases, and in cases in which the same peak was detected in both versions of the power spectrum, all peaks are shown in Figure 5, but they are combined into a single unweighted mean in Figure 6 and Table 1 (the uncertainties given in the table are discussed in § 4). We have been

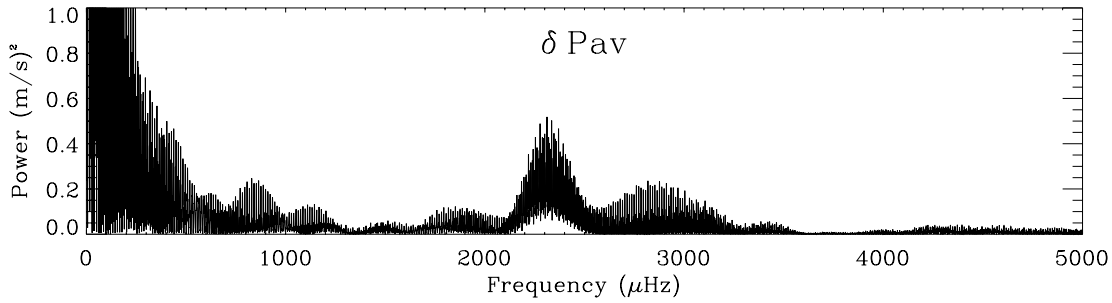


Fig. 3.—Power spectrum of velocity measurements of δ Pav from UVES and UCLES. There is a clear power excess at 2–3 mHz.

conservative in not selecting three peaks outside the main region because we cannot be sure of the curvature of the extrapolated ridge lines. These are 2827.7 μHz ($l = 0?$), 5894.9 μHz ($l = 2?$), and 5973.1 μHz ($l = 1?$).

Inspection of Figure 4 shows some apparent mismatches between the peaks in the power spectrum and the dotted lines representing the extracted frequencies. For example, there are enhancements in power at 3600, 3700, and 4050 μHz that do not correspond to identified modes. We noted similar structures in our analysis of α Cen A (Bedding et al. 2004), and the explanation is the same: the interaction of the window function with noise peaks and oscillation peaks. We have verified that the same phenomenon occurs in solar data by analyzing segments of the

publicly available⁷ 805 day series of full-disk velocity observations taken by the GOLF instrument (Global Oscillations at Low Frequencies) on the *Solar and Heliospheric Observatory (SOHO)* spacecraft (Ulrich et al. 2000; García et al. 2005), which have a sampling time of 80 s. We applied the same sampling window as used for our observations of α Cen B, and the results showed low-level structure in the power spectrum similar to those in Figure 4. This confirms that such a structure is a natural consequence of the spectral window interacting with multimode oscillations having finite lifetimes.

⁷ See <http://golfwww.medoc-ias.u-psud.fr>.

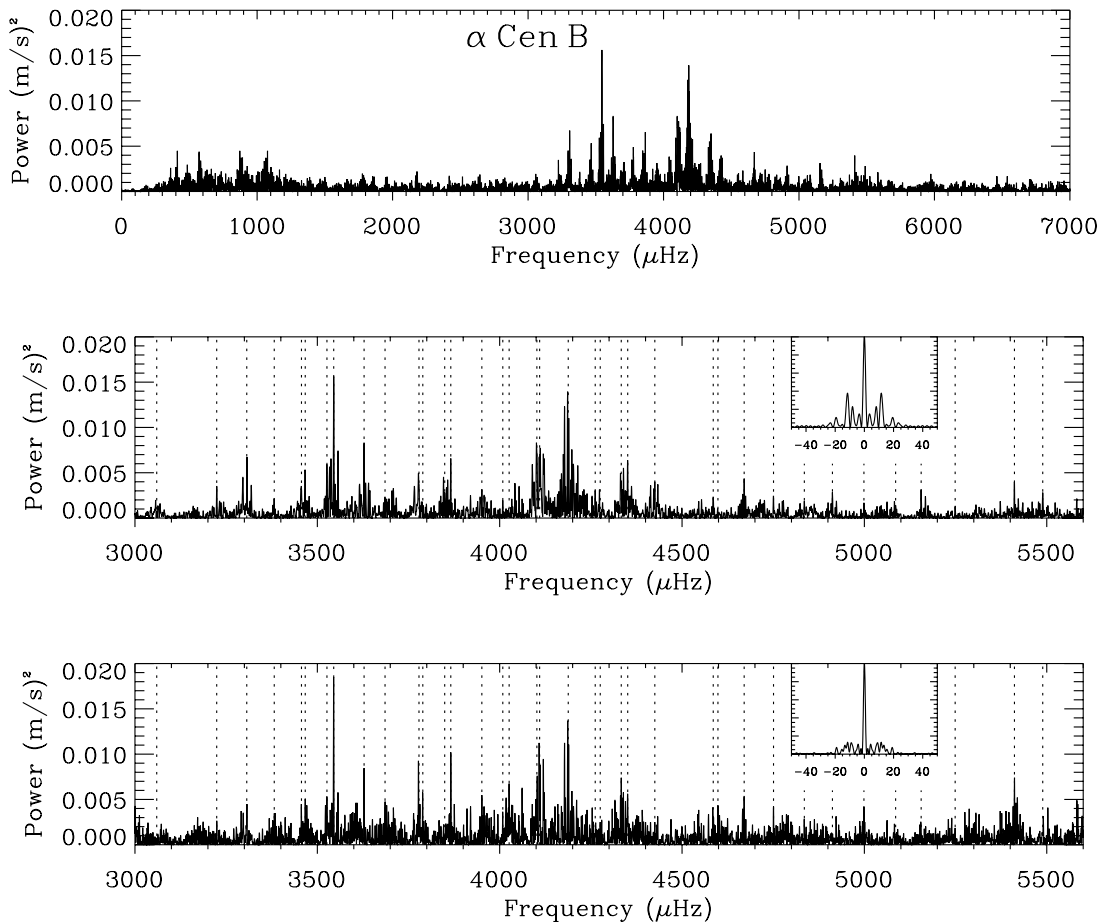


Fig. 4.—Power spectrum of α Cen B from the combined UVES and UCLES data. *Top*: Noise-optimized power spectrum, in which weights were based on the measurement uncertainties, which minimizes the noise. *Middle*: Same as top, but expanded to show only the central region. *Bottom*: Sidelobe-optimized power spectrum, in which weights were adjusted to minimize the aliases. The spectral windows are shown as insets, and vertical dotted lines show our final oscillation frequencies, as listed in Table 1.

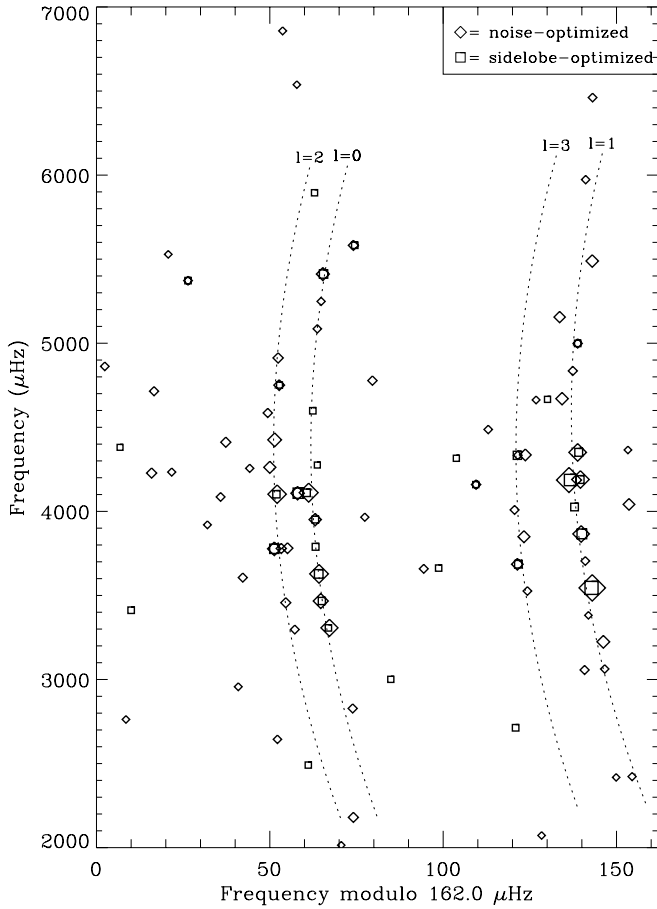


FIG. 5.—Peaks extracted by iterative sine wave fitting to the α Cen B power spectra, displayed in echelle format. Diamonds and squares, respectively, show peaks extracted from the noise-optimized and sidelobe-optimized power spectra. Symbol sizes are proportional to the S/N of the peaks. The dotted curves are fits to the final frequencies, given by eqs. (2)–(5).

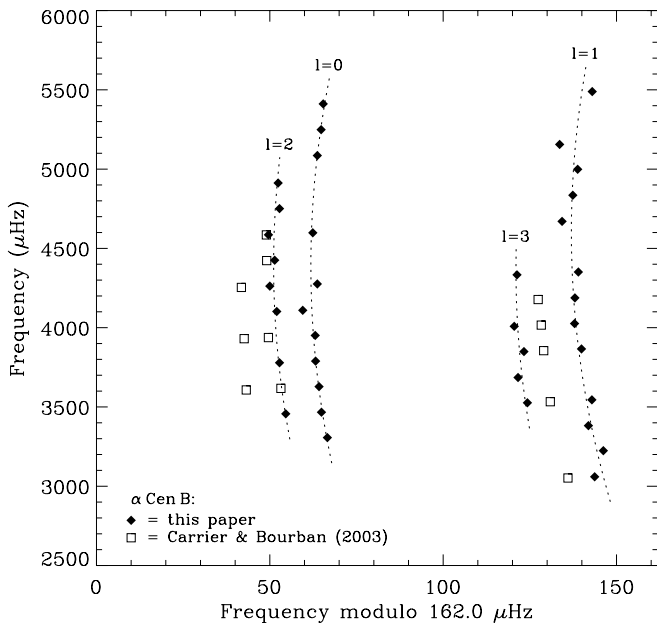


FIG. 6.—Echelle diagram of the final oscillation frequencies in α Cen B (filled diamonds), as listed in Table 1. Dotted curves show the fits to the frequencies, given by eqs. (2)–(5). Squares indicate the frequencies reported by Carrier & Bourban (2003).

TABLE 1
OSCILLATION FREQUENCIES FOR α CENTAURI B (μHz)

n	$l = 0$	$l = 1$	$l = 2$	$l = 3$
17.....	...	3059.7 ± 0.9
18.....	...	3224.2 ± 0.9
19.....	3306.6 ± 0.9	3381.9 ± 1.1	3456.6 ± 1.1	3526.3 ± 1.1
20.....	3466.9 ± 1.0	3544.9 ± 0.8	...	3685.6 ± 1.1
21.....	3628.2 ± 1.0	...	3778.8 ± 1.1	3849.3 ± 1.3
22.....	3789.2 ± 1.2	3865.9 ± 1.1	...	4008.5 ± 1.5
23.....	3951.1 ± 1.2	4025.9 ± 1.2	4102.0 ± 1.2	...
24.....	4109.5 ± 1.1	4188.0 ± 1.1	4262.0 ± 1.5	4333.3 ± 1.4
25.....	4275.7 ± 1.5	4351.0 ± 1.4	4425.4 ± 1.5	...
26.....	4585.6 ± 1.8	...
27.....	4598.4 ± 1.6	4670.3 ± 1.7	4750.8 ± 1.8	...
28.....	...	4835.4 ± 2.0	4912.4 ± 2.0	...
29.....	...	4998.8 ± 1.9
30.....	5085.7 ± 2.2	5155.6 ± 2.1
31.....	5248.8 ± 2.4
32.....	5411.4 ± 1.9	5489.0 ± 2.3

In Figure 6 the squares show the frequencies reported by Carrier & Bourban (2003). It is clear that, while they found the correct large separation, there is a shift in their frequencies of 1 cycle per day ($11.57 \mu\text{Hz}$). This reflects the problem associated with single-site observations, especially when the peaks have low S/N.

As with α Cen A, we note a scatter of the peaks about the ridge lines that is much higher than expected from S/N considerations and which we interpret as being due to the finite lifetime of the modes. We therefore fit to the ridges, in order to obtain more accurate estimates for the eigenfrequencies of the star. In the case of α Cen A (Bedding et al. 2004) we fitted to the frequencies in a two-step process by first fitting the three small separations and then fitting a parabola to the individual frequencies. Here we adopted a simpler approach that gives almost identical results, in which we fitted directly to the frequencies (see Ulrich 1986). The nine fitted parameters specify the curvatures of the parabolas (one common value), the large separation at some reference frequency for each l -value (four values), and the absolute positions of the ridges (four values). The equations for this fit are

$$\nu_{n,0} = [3950.57 + 161.45 (n - 23) + 0.101 (n - 23)^2] \mu\text{Hz}, \quad (2)$$

$$\nu_{n,1} = [4026.23 + 161.28 (n - 23) + 0.101 (n - 23)^2] \mu\text{Hz}, \quad (3)$$

$$\nu_{n,2} = [4101.41 + 161.63 (n - 23) + 0.101 (n - 23)^2] \mu\text{Hz}, \quad (4)$$

$$\nu_{n,3} = [4171.13 + 161.76 (n - 23) + 0.101 (n - 23)^2] \mu\text{Hz}. \quad (5)$$

We show this fit as the dotted curves in Figures 5 and 6.

Figure 7 shows the small frequency separations (*top*), the D_0 parameter (*middle*) and the large separations ($\Delta\nu$; *bottom*), using the same definitions as Bedding et al. (2004). Thus, $\delta\nu_{02}$ is the separation between adjacent peaks with $l = 0$ and 2, and $\delta\nu_{13}$ is the separation between $l = 1$ and 3. The third small separation, $\delta\nu_{01}$, is the amount by which $l = 1$ modes are offset from the midpoint between the $l = 0$ modes on either side:

$$\delta\nu_{01} = \frac{1}{2}(\nu_{n,0} + \nu_{n+1,0}) - \nu_{n,1}. \quad (6)$$

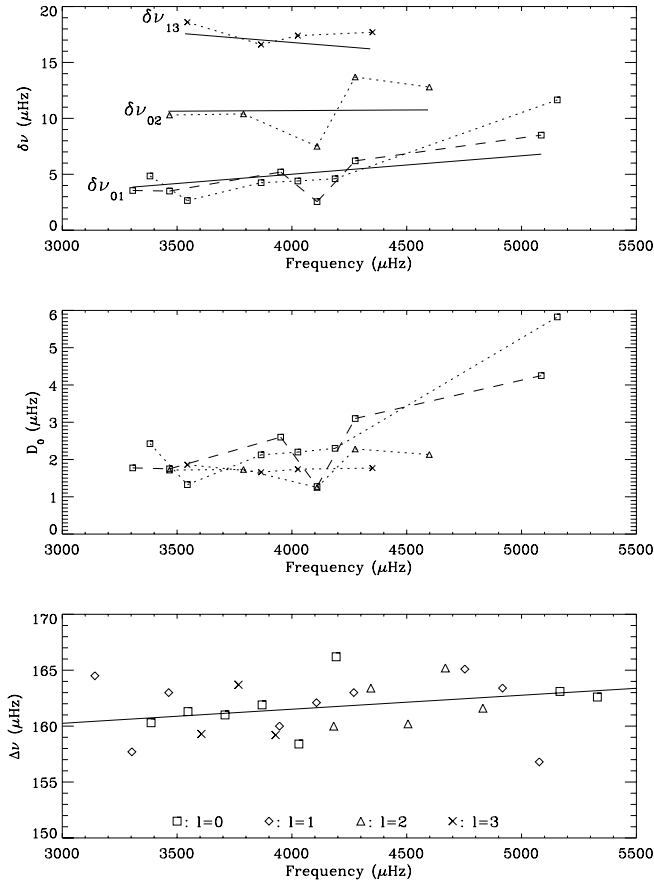


FIG. 7.—Frequency separations for α Cen B. *Top*: Small frequency separations, including $\delta\nu_{01}$ from both eqs. (6) and (7) (the dashed line connects the latter values). Solid lines show the separations calculated from eqs. (2)–(5). *Middle*: D_0 parameter, calculated as $(1/6)\delta\nu_{02}$, $(1/10)\delta\nu_{13}$, and $(1/2)\delta\nu_{01}$, with symbols (and line styles) showing the corresponding separations in the top panel. *Bottom*: Large separations for each value of l , with the solid line showing $\Delta\nu_0$ as calculated from eq. (2).

Since one could equally well define $\delta\nu_{01}$ to be the offset of $l = 0$ modes from the midpoint between consecutive $l = 1$ modes,

$$\delta\nu_{01} = \nu_{n,0} - \frac{1}{2}(\nu_{n-1,1} + \nu_{n,1}), \quad (7)$$

we have shown both versions in Figure 7 (*top*). Note that D_0 , which is sensitive to the stellar core, corresponds to $(1/6)\delta\nu_{02}$, $(1/10)\delta\nu_{13}$, and $(1/2)\delta\nu_{01}$ and is a constant if the asymptotic relation holds exactly. The solid lines in the top and bottom panels show the separations calculated from the fitted equations (in the bottom panel, only $\Delta\nu_0$ is shown; lines for other l -values are almost indistinguishable). The upward trend of $\Delta\nu$ with frequency is responsible for the curvature in the echelle diagram.

In Table 2 we give the large and small frequency separations for α Cen B at a frequency of 4.0 mHz. We also give ϵ , which is a dimensionless quantity commonly used to parameterize the absolute position of the frequency spectrum; see equation (1). We are not able to detect any statistically significant variations in the large separation with angular degree (l); the weighted mean value ($\Delta\nu$) has an uncertainty of 0.04%. We also find that the value of D_0 (as defined above) at 4.0 mHz is the same within the uncertainties for all three small separations, and our mean value for D_0 has an uncertainty of 3%. We can therefore place α Cen B in the so-called asteroseismic H-R diagram (Christensen-Dalsgaard

TABLE 2
FREQUENCY SEPARATIONS AT 4.0 mHz FOR α CENTAURI B (μ Hz)

Parameter	Value	%
$\Delta\nu_0$	161.50 ± 0.11	0.07
$\Delta\nu_1$	161.27 ± 0.09	0.06
$\Delta\nu_2$	161.48 ± 0.17	0.11
$\Delta\nu_3$	161.53 ± 0.33	0.20
$\Delta\nu$	161.38 ± 0.06	0.04
$\delta\nu_{01}$	4.52 ± 0.51	11
$\delta\nu_{02}$	10.14 ± 0.62	6
$\delta\nu_{13}$	16.73 ± 0.65	4
D_0	1.771 ± 0.047	3
ϵ	1.477 ± 0.011	

1984; see also Ulrich 1986; Gough 2003; Floranes et al. 2005), and these frequency separations should be compared with theoretical models.

Detailed modeling of the α Cen system was carried out by Eggenberger et al. (2004). They determined the parameters of the system through a least-squares fit to the observed quantities, including both “classical” photometric and spectroscopic data and oscillation frequencies from Bouchy & Carrier (2002) and Carrier & Bourban (2003). Their two preferred models (models M1 and M2) both have an age of 6.5 Gyr. For α Cen B they obtained large separations $\Delta\nu_0$ of 161.7 and 161.1 μ Hz, respectively, while the $l = 0-2$ small separations were $\delta\nu_{02} = 10.3$ and 10.2 μ Hz, respectively; both are essentially consistent with the values found here (see Table 2), although with some slight preference for model M1. It should be noted, however, that the average values of these quantities depend on the detailed way in which the averages are computed, including the selection of modes. Also, the computed values of $\Delta\nu_0$ and, to a lesser extent, $\delta\nu_{02}$ are affected by the uncertain physics of the near-surface layers of the model. An analysis of the combined set of frequencies for α Cen A, presented by Bedding et al. (2004), and the results of α Cen B shown in Table 1 is in progress.

3.1. Curvature at High and Low Frequencies

We now describe a method that allows us to measure the oscillations at low S/N, outside the central region in which we can identify individual modes. This allows us to examine curvature in the echelle diagram, which corresponds to measuring the large separation as a function of frequency. The method relies on smoothing the power spectrum in order to increase the contrast between the oscillation signal and the background noise. The first step was to smooth the power spectrum quite heavily, with a FWHM of $\Delta\nu/4$. This type of smoothing was used by García et al. (1998) to find high-frequency peaks in the solar power spectrum, but here we use an even broader smoothing function. The smoothing combines the power from each even-degree pair of modes ($l = 0$ and 2) into a single resolution element, and the same applies to the odd-degree pairs ($l = 1$ and 3).

We next arranged the smoothed power spectrum in echelle format, with frequencies reduced modulo $(1/2)\Delta\nu$ rather than the conventional $\Delta\nu$. This causes power associated with odd and even pairs to line up, allowing us to smooth in the vertical direction in this echelle diagram to improve the contrast further (for this smoothing we used $\text{FWHM} = 3.4\Delta\nu$). Finally, we measured the highest peak in each half-order, and these are marked by the open circles in Figure 8. We see a clear ridge of power that extends well beyond the central region. The dotted lines are the fits shown in Figure 6 and given by equations (2)–(5). We see

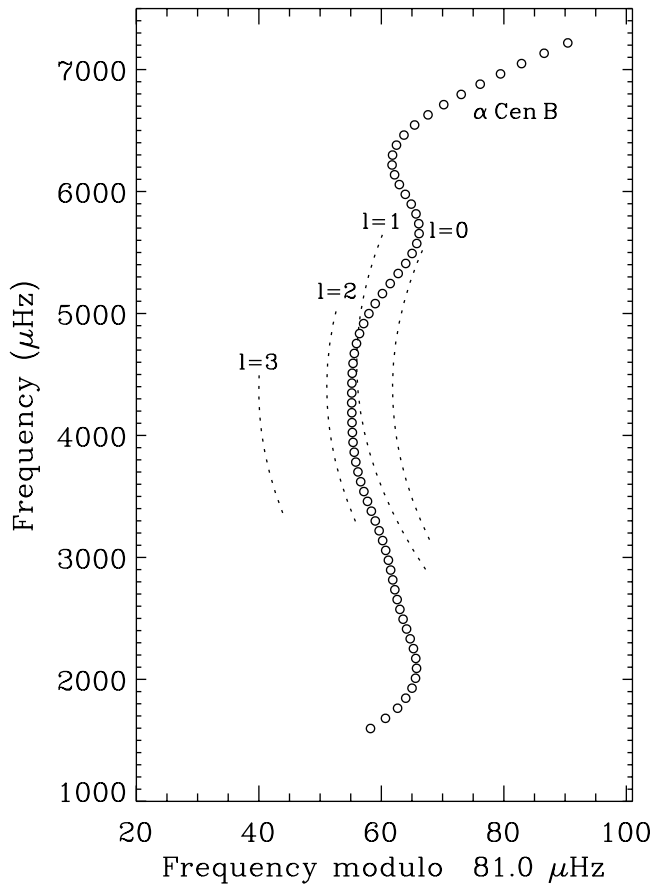


FIG. 8.—Smoothed echelle diagram of the power spectrum of α Cen B, plotted with frequencies reduced modulo half the large separation (see § 3.1 for details). The dotted lines correspond to the fits shown in Fig. 6 and given by eqs. (2)–(5).

good agreement in the central region, but the smoothed data allow us to measure curvature well outside the region in which we were able to identify individual oscillation modes.

In order to evaluate this method, we have also applied it to the oscillations in the Sun by analyzing the 805 day GOLF series (see § 3). We used the same amount of smoothing as for α Cen B (when specified in terms of $\Delta\nu$), and the filled circles in Figure 9 show the highest peaks in each half-order. The figure also shows published solar frequencies for $l = 0$ –3 (Lazrek et al. 1997; Bertello et al. 2000; Chaplin et al. 2002). We see that the ridge of power follows the published frequencies very well, but again extends beyond them at high frequencies. It is interesting that our measurements at high frequency match up perfectly with the so-called pseudomodes, also called HIPs (high-frequency interference peaks), which have been seen in smoothed solar power spectra up to 7.5 mHz (García et al. 1998; Chaplin et al. 2001; Gelly et al. 2002). This may be relevant to the discussion of the physical nature of these HIPs: are they related to ordinary resonant p -modes, despite having frequencies above the acoustic cutoff frequency in the atmosphere, caused by small but nonzero reflectivity at the photosphere (Balmforth & Gough 1990), or are they resonances between direct and reflected waves from a localized source (e.g., Kumar et al. 1990; Kumar & Lu 1991)?

The circles in Figure 10 show the large separation as a function of frequency for both α Cen B and the Sun. These values were derived from Figures 8 and 9, respectively, simply by doubling the differences between consecutive points along the ridges. The two curves are remarkably similar, except for the pronounced

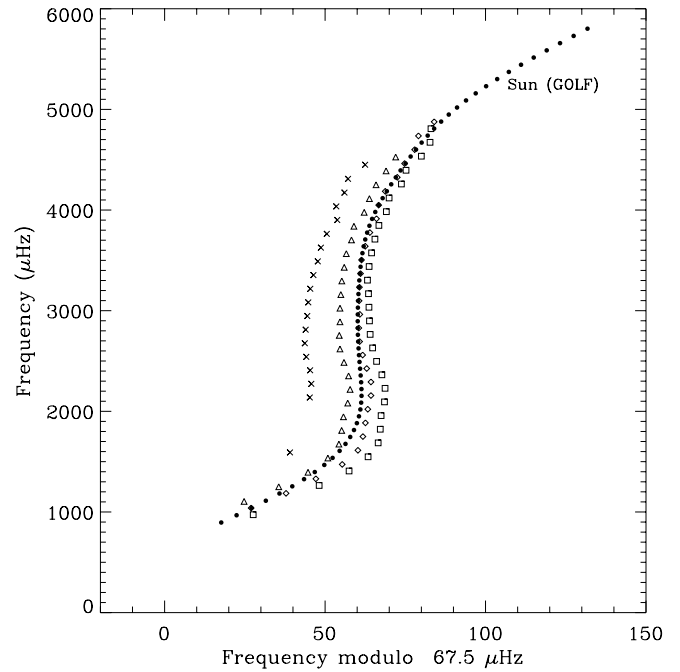


FIG. 9.—Similar to Fig. 8, but for a 805 day series of GOLF observations of the Sun. The open symbols are published solar frequencies for different l -values (open symbols have the same meaning as in Fig. 7, bottom).

dip at 6 mHz in α Cen B, which occurs in the region of low S/N and which we suspect is not real. In fact, our tests show that this type of feature sometimes appears as an artifact when the method is applied to short segments of the solar GOLF data (to match the observing window of α Cen B). The same tests also show that the method does measure $\Delta\nu$ very accurately in the regions where oscillations have significant amplitude. To illustrate this, the dashed lines in Figure 10 show our best estimates, based on these tests, of the $\pm 1 \sigma$ uncertainties in $\Delta\nu$. We conclude that this is a powerful technique for measuring the large separation over an extended frequency range. For α Cen B this will provide

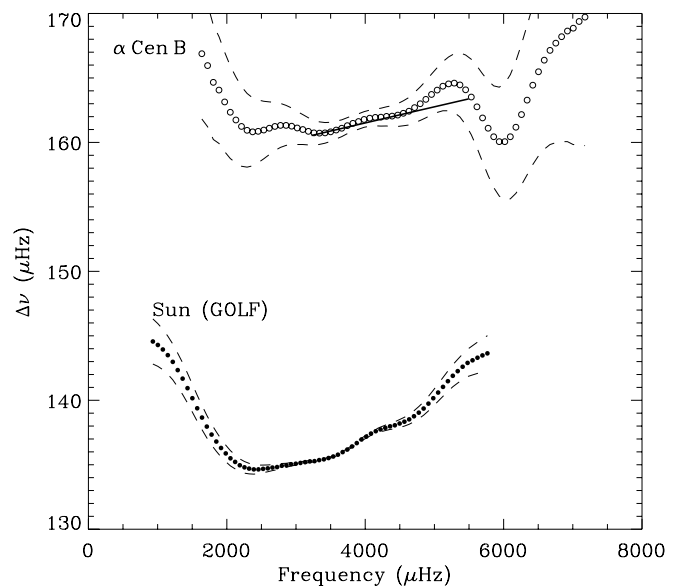


FIG. 10.—Large separation as a function of frequency in α Cen B and the Sun, as derived from Figs. 8 and 9. The dashed lines indicate the $\pm 1 \sigma$ uncertainties on $\Delta\nu$ (see text). The solid line for α Cen B is the same as Fig. 7 (bottom) and shows $\Delta\nu_0$ as calculated from eq. (2).

extra constraints on theoretical models while, for the Sun, we have been able to measure $\Delta\nu$ to much higher frequencies than has been done previously. The S-shaped structure in the echelle diagram indicates a departure from the second-order fit used in equations (2)–(5), implying that cubic (or higher) terms are needed to describe the frequencies fully. As pointed out by Ulrich (1988), these higher order coefficients might be useful in constraining the stellar mass.

4. MODE LIFETIMES

The scatter of the observed frequencies about the ridges allows us to estimate the mode lifetimes. In the case of α Cen A we did this by measuring the deviations of the measured frequencies from the fitted relations and comparing with simulations (Bedding et al. 2004). Here we adopted a slightly different approach that has the advantage of being independent of the fit, although it does still assume that we have correctly assigned n - and l -values. For each measured frequency $\nu_{n,l}$ (Fig. 6, *filled symbols*), except those at the ends of the ridges, we calculated the difference $\Delta_{n,l}$ between the measured frequency and that expected from the positions of the two nearest neighbors on the same ridge, using linear interpolation:

$$\Delta_{n,l} = \nu_{n,l} - \frac{\Delta n_- \nu_{(n+\Delta n_+),l} + \Delta n_+ \nu_{(n-\Delta n_-),l}}{\Delta n_+ + \Delta n_-}, \quad (8)$$

where the two neighboring modes lie in orders $n+\Delta n_+$ and $n-\Delta n_-$, respectively. In most cases, Δn_- and Δn_+ are 1, but in some cases one or both is 2 or even 3. We therefore need to convert $\Delta_{n,l}$ to a quantity that we can easily compare with simulations. We choose this to be the rms scatter of that peak about its expected position, calculated as follows:

$$\sigma_{n,l}^2 = \frac{(\Delta_{n,l})^2 (\Delta n_- + \Delta n_+)^2}{(\Delta n_- + \Delta n_+)^2 + (\Delta n_-)^2 + (\Delta n_+)^2}. \quad (9)$$

Averaging σ over many peaks gives an estimate of the mode lifetime, but we must keep in mind that the finite S/N also introduces a scatter to the peak positions. To calibrate these two contributions, we carried out a large number of simulations (175,000), each with a single input frequency and each sampled with our observational window function (with the noise-optimized weights). We used the method described by Stello et al. (2004) to generate the time series of an oscillation that was reexcited continuously with random kicks and damped on a timescale that was an adjustable parameter (the mode lifetime). The other adjustable input parameter was the oscillation amplitude, while the mode frequency and the noise level were fixed. We made 100 simulations for each set of input parameters, and from the resulting power spectra we measured the rms scatter in frequency of the highest peak and its mean S/N (discarding peaks with frequencies more than 4σ from the actual value). We repeated this for various values of the input parameters, and the results are summarized in Figure 11. Each solid line in this figure shows the observed frequency scatter versus the observed S/N for a given value of the mode lifetime. As expected, the frequency scatter increases both with decreasing mode lifetime and with decreasing S/N. We stress that this figure applies specifically to our observing window for α Cen B and should be recalculated for other observing windows.

The crosses in Figure 11 show our results for α Cen B in two frequency ranges, centered at 3.6 mHz (the mean of all peaks below 4.0 mHz) and at 4.6 mHz (the mean of peaks above 4.0 mHz). From these crosses we can determine the mode life-

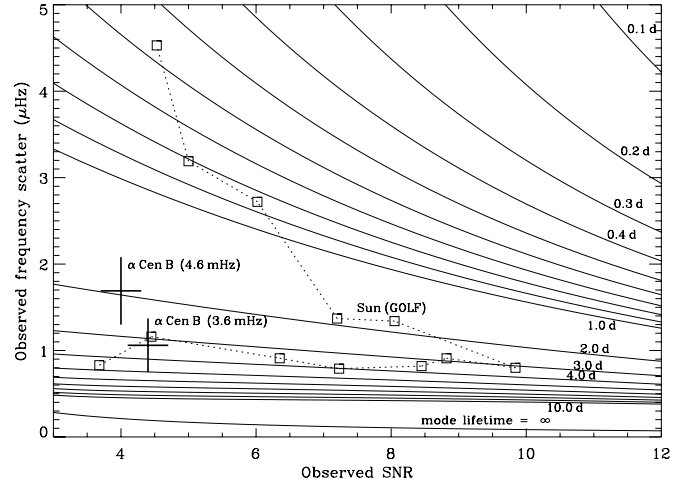


FIG. 11.—Calibration of mode lifetimes for the α Cen B observing window, using the noise-optimized weights. Solid lines are the results of simulations and show frequency scatter vs. S/N for various mode lifetimes. Crosses show actual results for α Cen B in two frequency ranges, while squares show results from GOLF data for 12 consecutive $l = 1$ modes in the Sun.

times. In order to check our results, we have also analyzed segments of the same 805 day GOLF series of full-disk velocity observations of the Sun used in § 3.1. We divided this series into 100 segments and imposed on each the α Cen B window function (with weights). The squares in Figure 11 show the frequency scatter for each $l = 1$ mode as a function of the mean S/N (both measured over the 100 segments). We analyzed 12 $l = 1$ modes ($n = 16$ –27) and ignored the pairs with $l = 0$ and 2 because they are less well resolved and interact via daily sidelobes. We see the well-known result that mode lifetimes in the Sun vary with frequency (the shortest lifetimes occur at the highest frequencies). Those with intermediate frequency have the best S/N because they have the highest amplitudes.

For each measured point in Figure 11 (two for α Cen B and 12 for the Sun), we used our simulations to infer the mode lifetime. The results are shown as a function of frequency in Figure 12 using the same symbols, where we have expressed frequency in

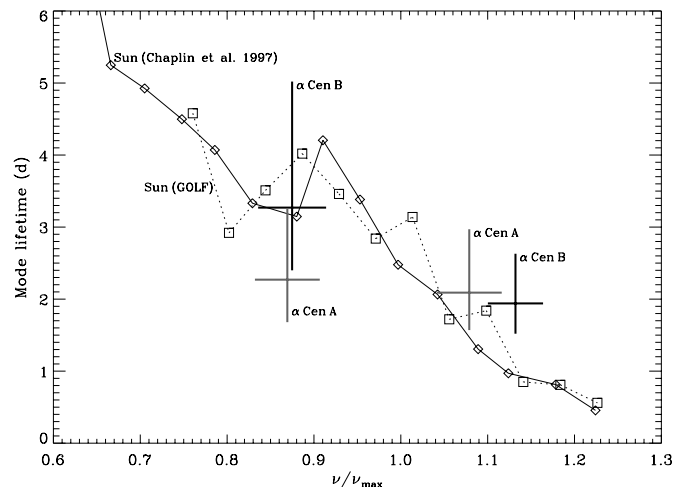


FIG. 12.—Mode lifetimes vs. normalized frequency, where ν_{\max} is the frequency of maximum oscillation power. Values for α Cen B (*black crosses*) and the Sun observed by GOLF (*squares*) are calculated from Fig. 11. Two values for α Cen A (*gray crosses*) are calculated from a similar calibration of the results presented by Bedding et al. (2004). Diamonds are published measurements of the solar mode lifetimes (Chaplin et al. 1997).

TABLE 3
AMPLITUDES AND NOISE LEVELS FOR SOLAR-LIKE OSCILLATIONS

STAR	SPECTROGRAPH	PEAK AMPLITUDE PER MODE (m s^{-1})	ν_{max} (mHz)	FWHM (mHz)	NOISE PER MINUTE (m s^{-1})	
					$2\nu_{\text{max}}$	11 mHz
α Cen B	UVES	0.085 ± 0.004	4.09 ± 0.17	1.98 ± 0.14	0.35	0.32
α Cen A	UVES	0.263 ± 0.008	2.41 ± 0.13	1.34 ± 0.04	0.49	0.45
β Hyi	UCLES	0.432 ± 0.016	1.02 ± 0.05	0.54 ± 0.05	2.47	...
δ Pav	UVES	0.236 ± 0.008	2.33 ± 0.09	1.24 ± 0.06	0.82	...
Sun	GOLF	0.308 ± 0.005	3.21 ± 0.11	1.76 ± 0.02	0.52	0.20
Sun	BiSON	0.233 ± 0.006	3.17 ± 0.13	1.62 ± 0.04	0.20	0.12
Sun	Lick	0.208 ± 0.029	2.95 ± 0.31

units of ν_{max} , the frequency of maximum oscillation power (see Table 3 for values of ν_{max}). The diamonds in this figure are published measurements of the solar mode lifetimes (Chaplin et al. 1997), and we see good agreement with our values. We also see that the typical mode lifetimes for α Cen B, when considered as a function of ν/ν_{max} , are similar to those in the Sun. Our estimates are $3.3_{-0.9}^{+1.8}$ days at 3.6 mHz and $1.9_{-0.4}^{+0.7}$ days at 4.6 mHz.

4.1. Revised Mode Lifetimes for α Cen A

The gray crosses in Figure 12 show mode lifetimes for α Cen A, based on the observations analyzed by Bedding et al. (2004). Here we have remeasured the mode lifetimes using the method described above, which involved making a whole new series of simulations with the α Cen A window function in order to convert frequency scatters into lifetimes. The inferred lifetimes are $2.3_{-0.6}^{+1.0}$ days at 2.1 mHz and $2.1_{-0.5}^{+0.9}$ days at 2.6 mHz.

We can compare these revised lifetimes for α Cen A with those we reported previously from the same data (see Table 3 in Bedding et al. 2004), $1.4_{-0.4}^{+0.5}$ days at 2.1 mHz and $1.3_{-0.4}^{+0.5}$ days at 2.6 mHz. The revised values are higher, although the 1σ error bars do overlap. The reason for the change is that our previous calculation underestimated the contribution of S/N to the frequency scatter. We did, of course, include the effects of S/N, but did so by treating it as being independent of the scatter introduced by finite mode lifetimes. In fact, as our new simulations show, the two contributions are not independent. If they were, the curves in Figure 11 would not rise toward low S/N as steeply as they do.

The important conclusion, as we can see from Figure 12, is that mode lifetimes in α Cen A are not substantially lower than those in the Sun, although the value for the lower frequency range is still about 1.5σ below solar.

5. AMPLITUDES AND NOISE LEVELS

It is important to measure oscillation amplitudes in solar-like stars and to compare these with theoretical calculations (e.g., Houdek et al. 1999). It is also interesting to measure the background noise from stellar convection, although in velocity this requires extremely precise measurements because the signature is weak. For both these measurements, we have chosen to smooth the power spectrum heavily, so as to produce a single hump of excess power that is insensitive to the fact that the oscillation spectrum has discrete peaks. It is also useful to convert to power density, which is independent of the observing window and therefore allows us to compare noise levels. This is done by multiplying the power by the effective length of the observing run, which we calculated as the reciprocal of the area under the spectral window (in power).

In Figure 13 we show smoothed power density spectra for the Sun and four other stars: α Cen A and B, δ Pav, and β Hyi. For the four stars, we used the most precise observations available: UVES observations for α Cen B (this paper), δ Pav (this paper), and α Cen A (Butler et al. 2004) and UCLES observations for β Hyi (Bedding et al. 2001). In all cases we used the raw velocity measurements, before removal of any jumps or slow trends, since we are interested in measuring the total noise level.

For the Sun, we used data from BiSON (Birmingham Solar Oscillations Network) and GOLF. The BiSON data comprised a 7 day time series with 40 s sampling from the Las Campanas station in Chile, kindly provided by W. Chaplin (2003, private communication). The GOLF data comprised a 20 day time series with 20 s sampling, kindly provided by P. Boumier (2004, private communication). Note that these have a higher Nyquist frequency than the publicly available GOLF data, which we used in §§ 3.1 and 4 but which are only sampled at 80 s.

The dotted lines in Figure 13 are fits to the noise backgrounds, based on the Harvey (1985) model of solar granulation. The Harvey model gives a convenient functional form, even in stars in which the low-frequency noise has a strong additional contribution from instrumental noise. We discuss the noise levels in more detail below. First, we show that these smoothed power density spectra provide a powerful way to measure oscillation amplitudes in a way that is independent of mode lifetime.

To do this, we first subtracted the background noise (Fig. 13, dotted lines) from each observed power density spectrum. We

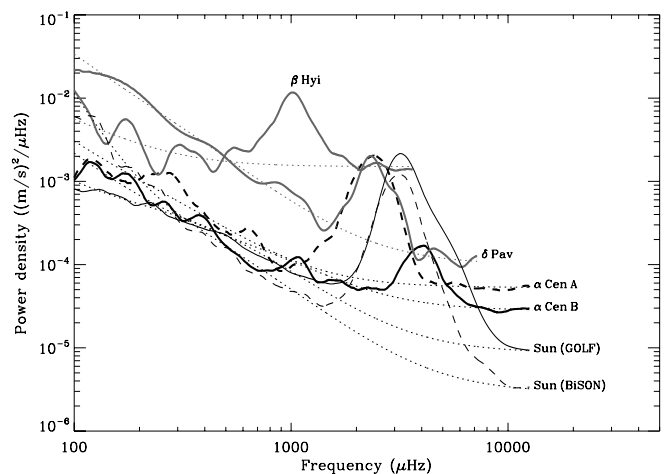


FIG. 13.—Smoothed power density spectra from velocity observations of the Sun and four other stars. The dotted lines are fits to the noise background.

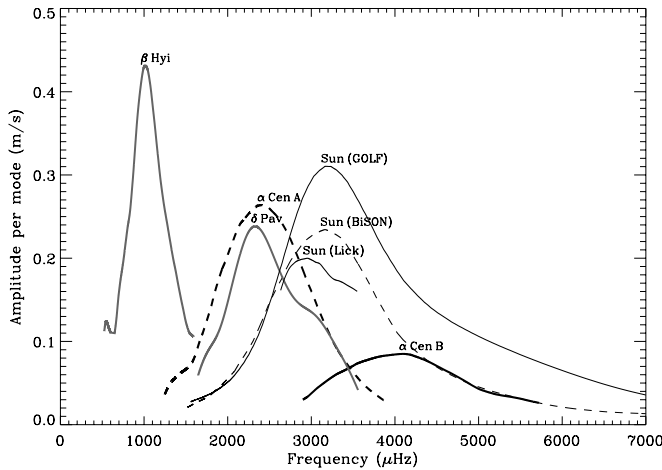


FIG. 14.—Amplitude per mode for solar-like oscillations. These curves were calculated from those in Fig. 13 by subtracting the background noise, multiplying by $\Delta\nu/3.0$, and taking the square root (see text). We also show oscillation amplitudes in the Sun, measured from iodine-referenced observations at Lick Observatory.

only included those parts of the spectrum that were at least twice the noise level. In order to calculate the amplitude per oscillation mode, we should then multiply by $\Delta\nu/4$ (where $\Delta\nu$ is the large frequency separation of the star) and take the square root. The rationale for this is that there are four modes in each segment of length $\Delta\nu$ (with $l = 0, 1, 2,$ and 3). However, we must keep in mind that modes with different angular degrees have different visibilities in full-disk observations, due to varying amounts of cancellation. Based on the results presented by Bedding et al. (1996), we calculated the effective number of modes per $\Delta\nu$, normalized to the mean of the $l = 0$ and 1 amplitudes, to be 3.0 . We therefore used this factor, rather than 4 , in our calculation.

For $\Delta\nu$ we used the following values: $135 \mu\text{Hz}$ for the Sun, $106 \mu\text{Hz}$ for α Cen A, $162 \mu\text{Hz}$ for α Cen B, $56 \mu\text{Hz}$ for β Hyi, and $93 \mu\text{Hz}$ for δ Pav. The last of these is not a measurement, since none is available, but is instead derived from the following adopted parameters: $M = 0.9 M_{\odot}$, $L = 1.3 L_{\odot}$, and $T_{\text{eff}} = 5540 \text{ K}$.

Our amplitude estimates are shown in Figure 14, and the height, frequency, and FWHM of the envelopes are given in Table 3. We see a number of interesting things from Figures 13 and 14. Looking first at the Sun, the results illustrate very nicely that the solar oscillation amplitude depends on the spectral line that is being measured (see Baudin et al. [2005] for a recent study of this phenomenon). The sodium line used by GOLF is formed higher in the solar atmosphere than the potassium line used by BiSON, which is why GOLF measures higher oscillation amplitudes (Isaak et al. 1989). The actual height difference is difficult to estimate; Palte et al. (1992) quoted $\sim 200 \text{ km}$, while Baudin et al. (2005) adopted $\sim 60 \text{ km}$. Velocity measurements of other stars are made using a wide wavelength range so as to include many spectral lines, and the Doppler signal is dominated by neutral iron lines. Since these lines are formed about 400 km below the sodium D lines (Eibe et al. 2001; Meunier & Kosovichev 2003), we would expect solar amplitudes measured using the iodine technique to be less than those from both BiSON and GOLF.

Unfortunately, there do not appear to be any published estimates of the solar oscillation amplitude using the stellar technique. Here we present some previously unpublished observations of the

solar spectrum made using iodine referencing. One of us (J. T. W.) made observations of the Moon using the 0.6 m Coude Auxilliary Telescope (CAT) at Lick Observatory, which fed the Hamilton Spectrometer, a high-resolution ($R = 60,000$) echelle (Vogt 1987). The CAT tracked a fixed point of uniform surface brightness (Archimedes crater) for five consecutive nights near full moon, thus measuring the disk-integrated solar spectrum at night (a technique inspired by McMillan et al. 1993). These velocity measurements allowed us to estimate the solar oscillation amplitude, which we include in Figure 14 and Table 3. The results support the conclusion that Fe I measurements give lower amplitudes than both GOLF and BiSON. They also place the solar amplitude between those of α Cen A and B, as would be expected given their stellar parameters. It would clearly be valuable to obtain more measurements of the Sun, in order to better calibrate the relationship between stellar and solar amplitudes. The method described here allows us to estimate amplitudes independently of mode lifetime and observing window. Comparing the amplitudes of different stars with theoretical models is the subject of a future paper.

We turn now to the noise levels in the various observations, looking first at low frequencies. The rise in power toward low frequencies seen in Figure 13 is due to a combination of instrumental drift and stellar background noise. Of course, it is very difficult to distinguish between these two, although in the Sun it is established that the solar background is dominant. It therefore seems likely that the low-frequency power from α Cen A is also mostly stellar, given that the power density is similar to that of the Sun (see also Kjeldsen et al. 1999). The same may also be true for α Cen B. We can certainly say that at 1 mHz , the granulation noise in both stars is no greater than is observed in the Sun by GOLF and BiSON.

At the highest frequencies the noise levels are dominated by white noise from photon statistics. We can see that the power density (which indicates noise per unit observing time) is lowest for BiSON and GOLF, followed by α Cen B (UVES) and α Cen A (UVES). In the last two columns of Table 3 we provide an update to Table 1 of Butler et al. (2004), showing the noise per minute of observing at frequencies just above the p -mode envelope ($2\nu_{\text{max}}$) and also, where the sampling allows, at very high frequencies (11 mHz). We should note that the power at high frequencies in the Sun ($4\text{--}6 \text{ mHz}$), particularly in the sodium line used by GOLF, is dominated by solar noise that presumably arises from chromospheric effects, with only a small fraction being due to coherent p -modes.

6. CONCLUSIONS

Our observations of α Cen B from two sites have allowed us to identify 37 oscillation modes with $l = 0\text{--}3$. Fitting to these modes gave the large and small frequency separations as a function of frequency. We also introduced a new method, involving smoothing in the $(1/2)\Delta\nu$ echelle diagram, that allowed us to trace the ridges of power, and hence measure the large separation, well beyond the central region.

We inferred the mode lifetimes in two frequency ranges by measuring the scatter of the oscillation frequencies about a smooth trend, based on a calibration involving extensive simulations. We found mode lifetimes in α Cen B, when considered as a function of frequency relative to the maximum power, that are consistent with those seen in the Sun. We applied the same analysis to our observations of α Cen A and deduced revised mode lifetimes that are slightly higher than we previously published (Bedding et al. 2004).

A limited set of observations of the star δ Pav showed oscillations centered at 2.3 mHz with peak velocity amplitudes close to solar. Further observations are needed to determine the large separation and individual mode frequencies in this star.

Finally, we also introduced a new method of measuring oscillation amplitudes from heavily smoothed power density spectra. We estimated the amplitude per mode of α Cen A and B, β Hyi, δ Pav, and the Sun and pointed out that the results may depend on which spectral lines are used for the velocity measurements.

We thank the GOLF team for providing the data at 20 s sampling, and we are grateful to Alan Gabriel and Patrick Boumier for useful comments. We also thank Bill Chaplin for providing data from BiSON and for useful discussions. This work was supported financially by the Australian Research Council, by the Danish Natural Science Research Council, and by the Danish National Research Foundation through its establishment of the Theoretical Astrophysics Center. We further acknowledge support by NSF grant AST 99-88087 (R. P. B.), and by SUN Microsystems.

REFERENCES

- Balmforth, N. J., & Gough, D. O. 1990, *ApJ*, 362, 256
- Baudin, F., Samadi, R., Goupil, M.-J., Appourchaux, T., Barban, C., Boumier, P., Chaplin, W. J., & Gouttebroze, P. 2005, *A&A*, 433, 349
- Bedding, T. R., Kjeldsen, H., Butler, R. P., McCarthy, C., Marcy, G. W., O'Toole, S. J., Tinney, C. G., & Wright, J. T. 2004, *ApJ*, 614, 380
- Bedding, T. R., Kjeldsen, H., Reetz, J., & Barbuy, B. 1996, *MNRAS*, 280, 1155
- Bedding, T. R., et al. 2001, *ApJ*, 549, L105
- Bertello, L., Varadi, F., Ulrich, R. K., Henney, C. J., Kosovichev, A. G., & García, R. A. 2000, *ApJ*, 537, L143
- Bouchy, F., & Carrier, F. 2001, *A&A*, 374, L5
- . 2002, *A&A*, 390, 205
- Butler, R. P., Bedding, T. R., Kjeldsen, H., McCarthy, C., O'Toole, S. J., Tinney, C. G., Marcy, G. W., & Wright, J. T. 2004, *ApJ*, 600, L75
- Butler, R. P., Marcy, G. W., Williams, E., McCarthy, C., Dossanji, P., & Vogt, S. S. 1996, *PASP*, 108, 500
- Carrier, F., & Bourban, G. 2003, *A&A*, 406, L23
- Chaplin, W. J., Elsworth, Y., Isaak, G. R., Marchenkov, K. I., Miller, B. A., & New, R. 2001, in *Proc. SOHO 10/GONG 2000 Workshop: Helio- and Asteroseismology at the Dawn of the Millennium*, ed. A. Wilson (ESA SP-464; Noordwijk: ESA), 191
- Chaplin, W. J., Elsworth, Y., Isaak, G. R., Marchenkov, K. I., Miller, B. A., New, R., Pinter, B., & Appourchaux, T. 2002, *MNRAS*, 336, 979
- Chaplin, W. J., Elsworth, Y., Isaak, G. R., McLeod, C. P., Miller, B. A., & New, R. 1997, *MNRAS*, 288, 623
- Christensen-Dalsgaard, J. 1984, in *Workshop on Space Research in Stellar Activity and Variability*, ed. A. Manganey & F. Praderie (Meudon: Obs. Paris), 11
- Deeming, T. J. 1975, *Ap&SS*, 36, 137
- Eggenberger, P., Charbonnel, C., Talon, S., Meynet, G., Maeder, A., Carrier, F., & Bourban, G. 2004, *A&A*, 417, 235
- Eibe, M. T., Mein, P., Roudier, T., & Faurobert, M. 2001, *A&A*, 371, 1128
- Flaranes, H. O., Christensen-Dalsgaard, J., & Thompson, M. J. 2005, *MNRAS*, 356, 671
- Frandsen, S., Jones, A., Kjeldsen, H., Viskum, M., Hjorth, J., Andersen, N. H., & Thomsen, B. 1995, *A&A*, 301, 123
- García, R. A., et al. 1998, *ApJ*, 504, L51
- . 2005, *A&A*, 442, 385
- Gelly, B., Lazrek, M., Grec, G., Ayad, A., Schmider, F. X., Renaud, C., Salabert, D., & Fossat, E. 2002, *A&A*, 394, 285
- Gough, D. O. 2003, *Ap&SS*, 284, 165
- Harvey, J. W. 1985, in *ESA Future Missions in Solar, Heliospheric, and Space Plasma Physics* (ESA SP-235; Noordwijk: ESA), 199
- Houdek, G., Balmforth, N. J., Christensen-Dalsgaard, J., & Gough, D. O. 1999, *A&A*, 351, 582
- Isaak, G. R., McLeod, C. P., Pallé, P. L., van der Raay, H. B., & Roca Cortés, T. 1989, *A&A*, 208, 297
- Kjeldsen, H., Bedding, T. R., Frandsen, S., & Dall, T. H. 1999, *MNRAS*, 303, 579
- Kumar, P., Duvall, T. L., Harvey, J. W., Jefferies, S. M., Pomerantz, M. A., & Thompson, M. J. 1990, in *Proc. Oji Int. Seminar: Progress of Seismology of the Sun and Stars*, ed. Y. Osaki & H. Shibahashi (Berlin: Springer), 87
- Kumar, P., & Lu, E. 1991, *ApJ*, 375, L35
- Lazrek, M., et al. 1997, *Sol. Phys.*, 175, 227
- McMillan, R. S., Moore, T. L., Perry, M. L., & Smith, P. H. 1993, *ApJ*, 403, 801
- Meunier, N., & Kosovichev, A. 2003, *A&A*, 412, 541
- Palle, P. L., Regulo, C., Roca-Cortés, T., Sanchez-Duarte, L., & Schmider, F. X. 1992, *A&A*, 254, 348
- Stello, D., Kjeldsen, H., Bedding, T. R., De Ridder, J., Aerts, C., Carrier, F., & Frandsen, S. 2004, *Sol. Phys.*, 220, 207
- Ulrich, R. K. 1986, *ApJ*, 306, L37
- . 1988, in *IAU Symp. 123, Advances in Helio- and Asteroseismology*, ed. J. Christensen-Dalsgaard & S. Frandsen (Dordrecht: Kluwer), 299
- Ulrich, R. K., et al. 2000, *A&A*, 364, 799
- Vogt, S. S. 1987, *PASP*, 99, 1214